# Supporting Information

# Impact of the $F^-$ for $O^{2-}$ substitution in $Na_3V_2(PO_4)_2F_{3-y}O_y$ on their transport properties and electrochemical performance

Runhe Fang [a,d], Jacob Olchowka [b,d,e,*], Chloé Pablos [b,c,d], Rafael Bianchini Nuernberg [b], Laurence Croguennec [b,d,e], Sophie Cassaignon[a,d,*]

[a] Sorbonne Université, CNRS, Laboratoire Chimie de la Matière Condensée de Paris, LCMCP, UMR 7574, 4 Place Jussieu, 75005 Paris, France

[b] Univ. Bordeaux, CNRS, Bordeaux INP, ICMCB, UMR 5026, F-33600 Pessac, France

[c] Laboratoire de Réactivité et de Chimie des Solides, Université de Picardie Jules Verne, CNRS-UMR 7314, F-80039 Amiens Cedex 1, France

[d] RS2E, Réseau Français sur le Stockage Electrochimique de l'Energie, CNRS 3459, 80039 Amiens Cedex 1, France.

[e] ALISTORE-ERI European Research Institute, CNRS 3104, 80039 Amiens Cedex 1, France

* Corresponding authors:

S. Cassaignon (sophie.cassaignon@sorbonne-universite.fr)

J. Olchowka (jacob.olchowka@icmcb.cnrs.fr)

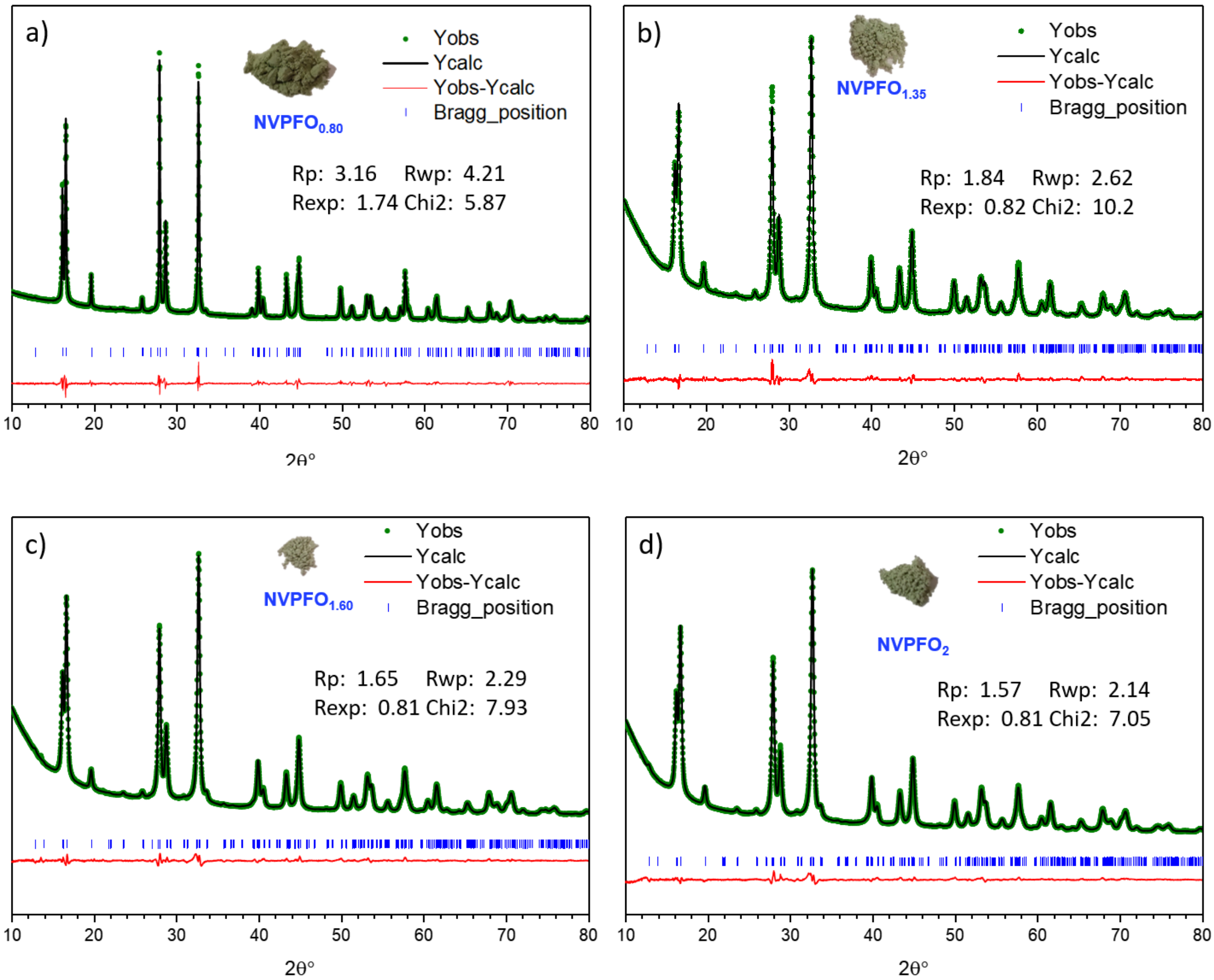


*Figure S1. Rietveld refinement of the XRD data for the different compounds $NVPFO_{0.80}$, $NVPFO_{1.35}$, $NVPFO_{1.60}$ and $NVPFO_2$.*

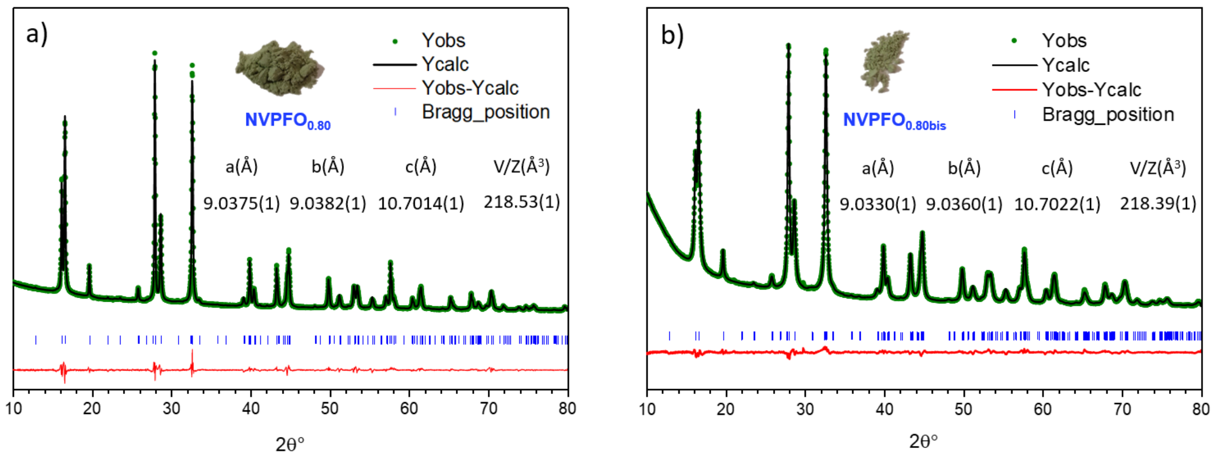


*Figure S2. The cell parameter comparison of the $NVPFO_{0.80}$ and $NVPFO_{0.80bis}$*

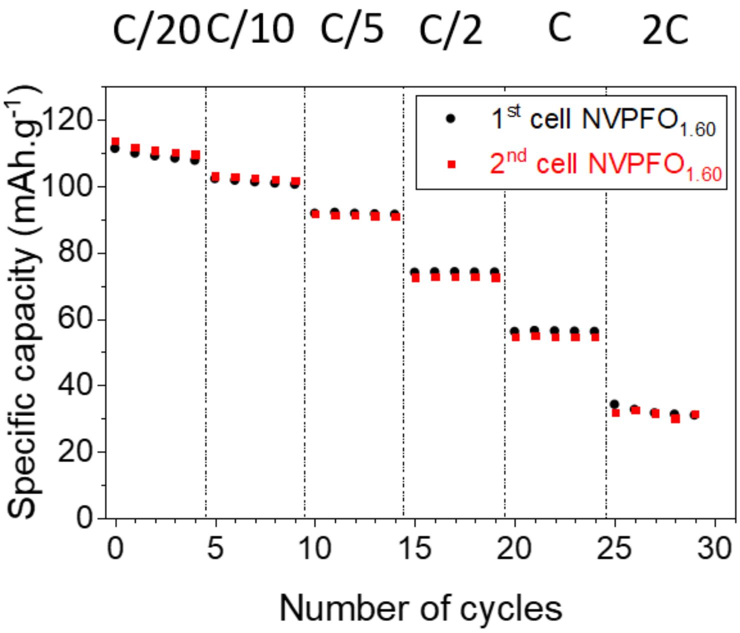


*Figure S3. Illustration of the reproducibility of the electrochemical performance obtained for NVPFO$_{1.6}$.*

This shows an example of the reproducibility of the electrochemical tests that were performed for NVPFO$_{1.6}$. The reproducibility tests validate that the different performance in the study are induced by the different chemical composition and not influenced by the experimental cell assembly.

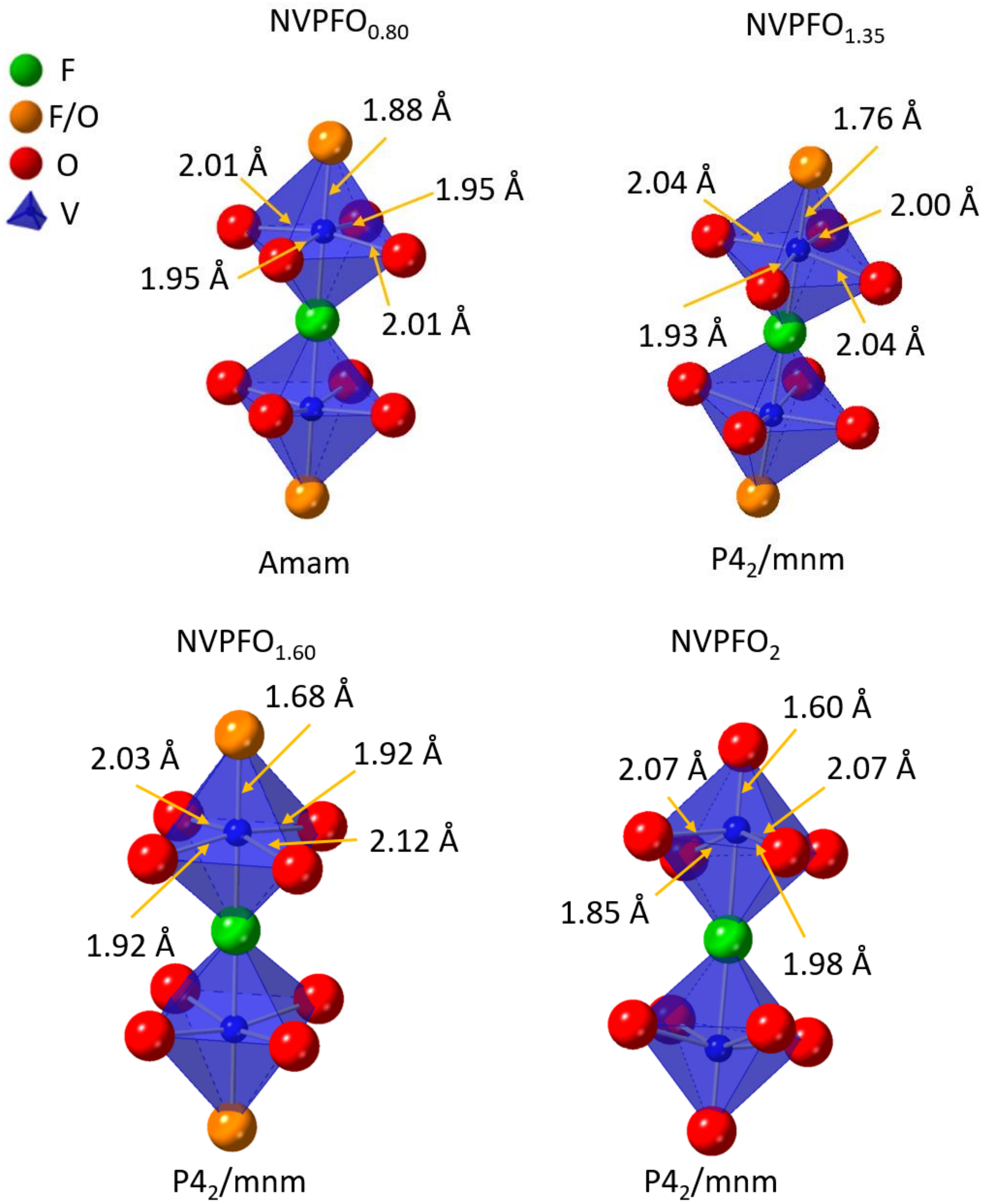


*Figure S4. Illustration of bond distance changes from the composition $NVPFO_{0.80}$ to the composition $NVPFO_2$.*

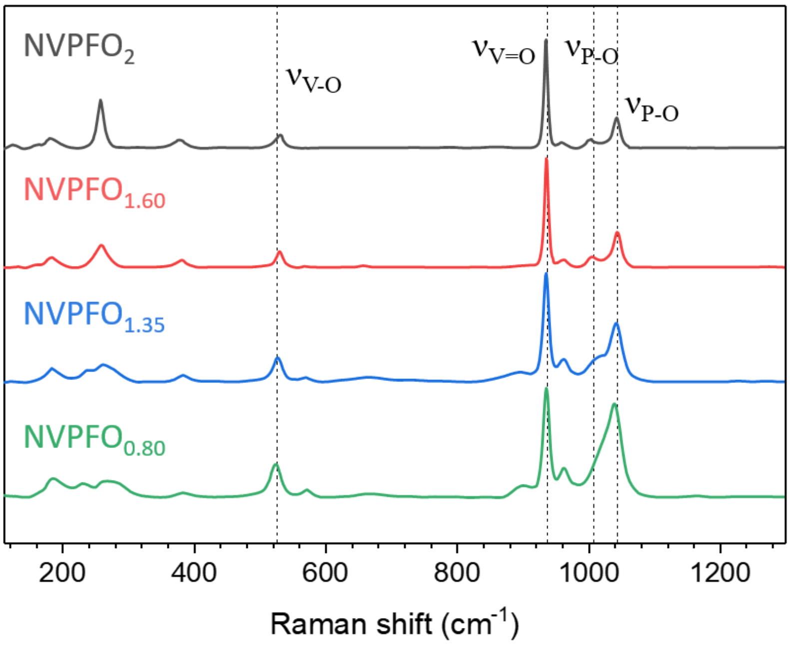


*Figure S5. All Raman spectra from 100 cm$^{-1}$ to 1300 cm$^{-1}$. The spectra were corrected to remove the background. The absence of signal after 1150 cm$^{-1}$ confirmed the absence of carbon in the compounds (absence of D-band, see Figure S6)*[1].

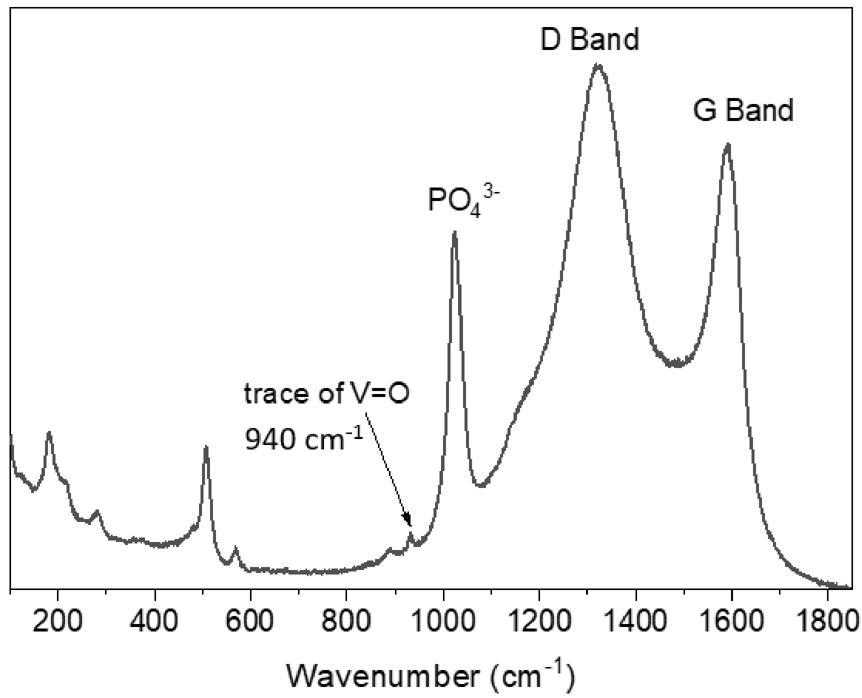


*Figure S6. Raman spectrum of carbon-coated $Na_3V_2(PO_4)_2F_3$ (y=0). The electrode material was synthesized through the method proposed by Hall et al.[2] This spectrum confirms the absence of carbon in the series studied in this work (absence of signal around 1150-1300 $cm^{-1}$ as shown in Figure S5) and endorses the attribution of the signal at 940 $cm^{-1}$ to vanadyl bond vibration since this signal nearly disappears for $Na_3V^{3+}{}_2(PO_4)_2F_3$. Indeed, as reported previously, a small amount of vanadyl type defects is always identified, which explains the detection of the signal at 940 $cm^{-1}$.[3]*

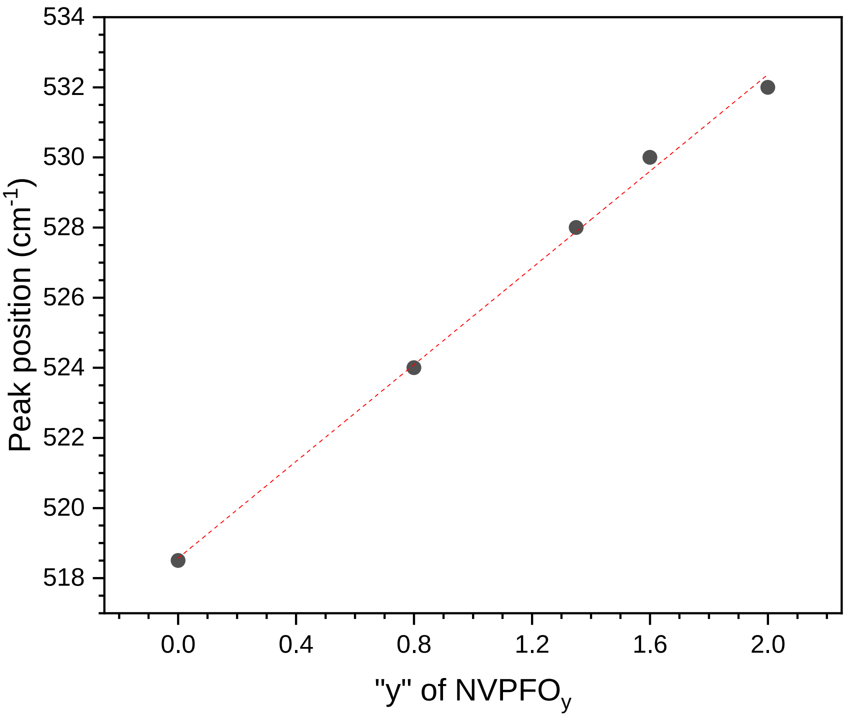


*Figure S7. "y" of $NVPFO_y$ variation versus the shift of the V-O peak position. The linear fitting in red clearly demonstrates a linear shift of the peak according to the chemical formulae. The position of V-O band for NVPF3 (y=0) is measured from the spectrum reported in figure S6.*

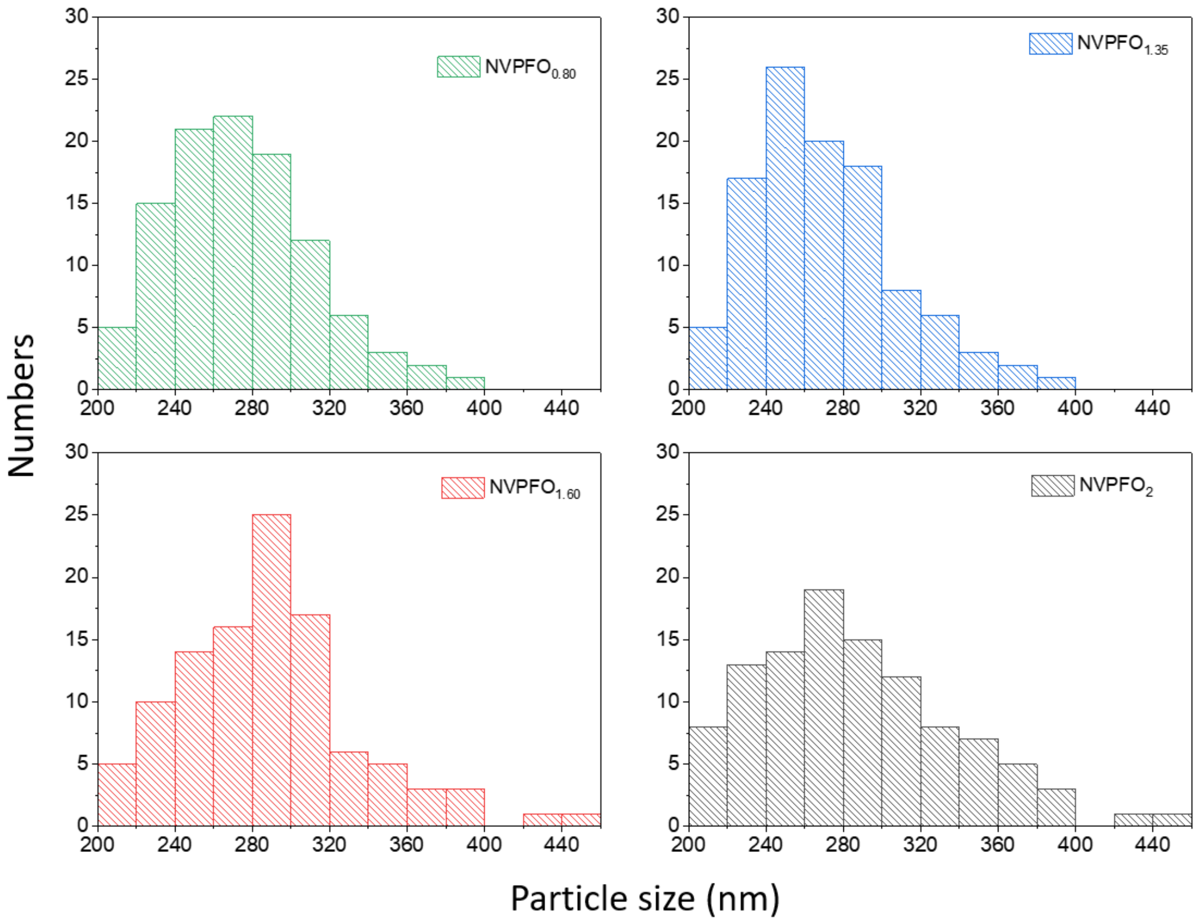


*Figure S8. Statistics of particle size distribution for all the materials. For each material 106 particles were measured.*

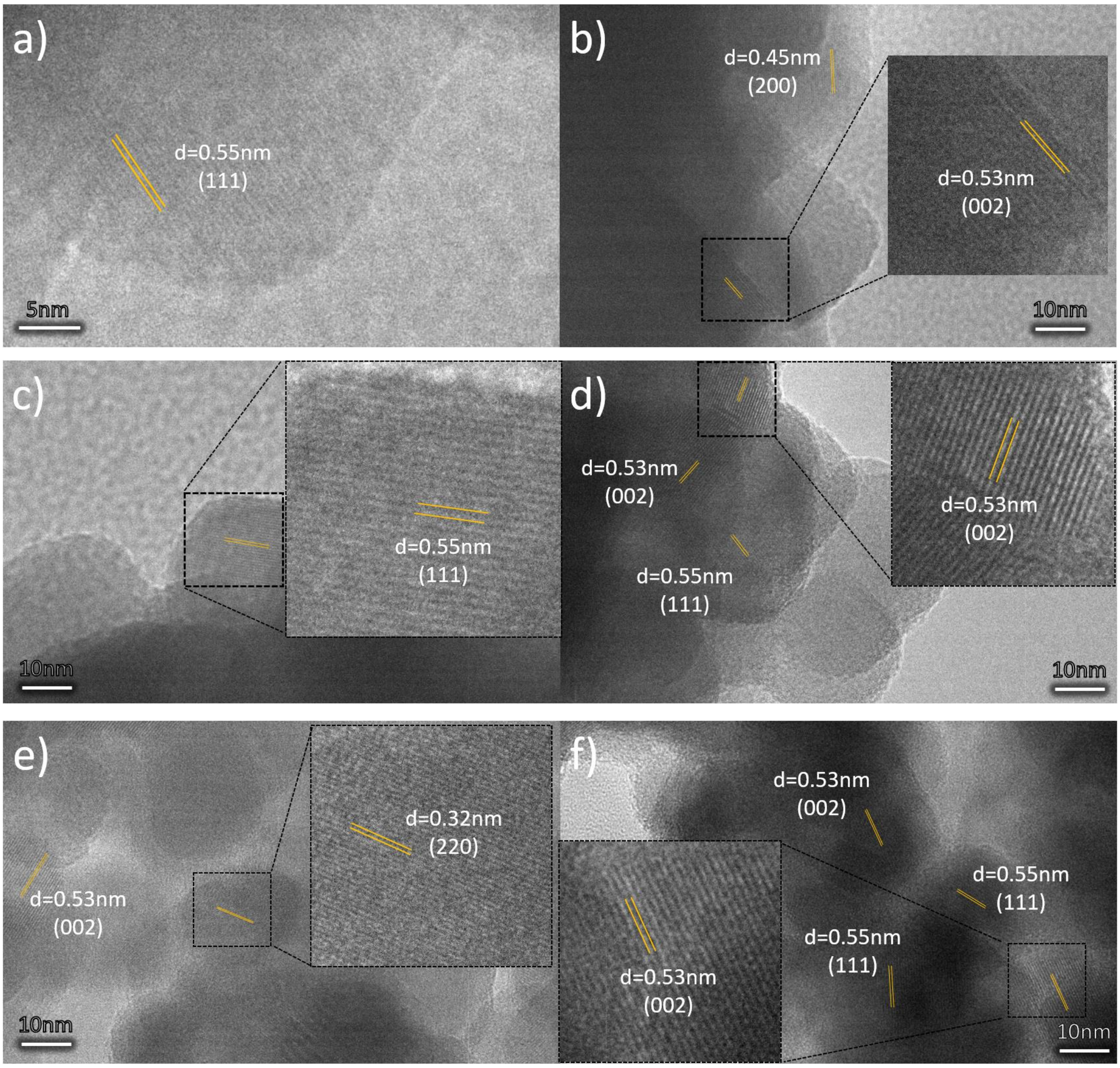


*Figure S9. HRTEM images of a-b) $NVPFO_{0.80}$, c-d) $NVPFO_{1.60}$ and e-f) $NVPFO_2$.*

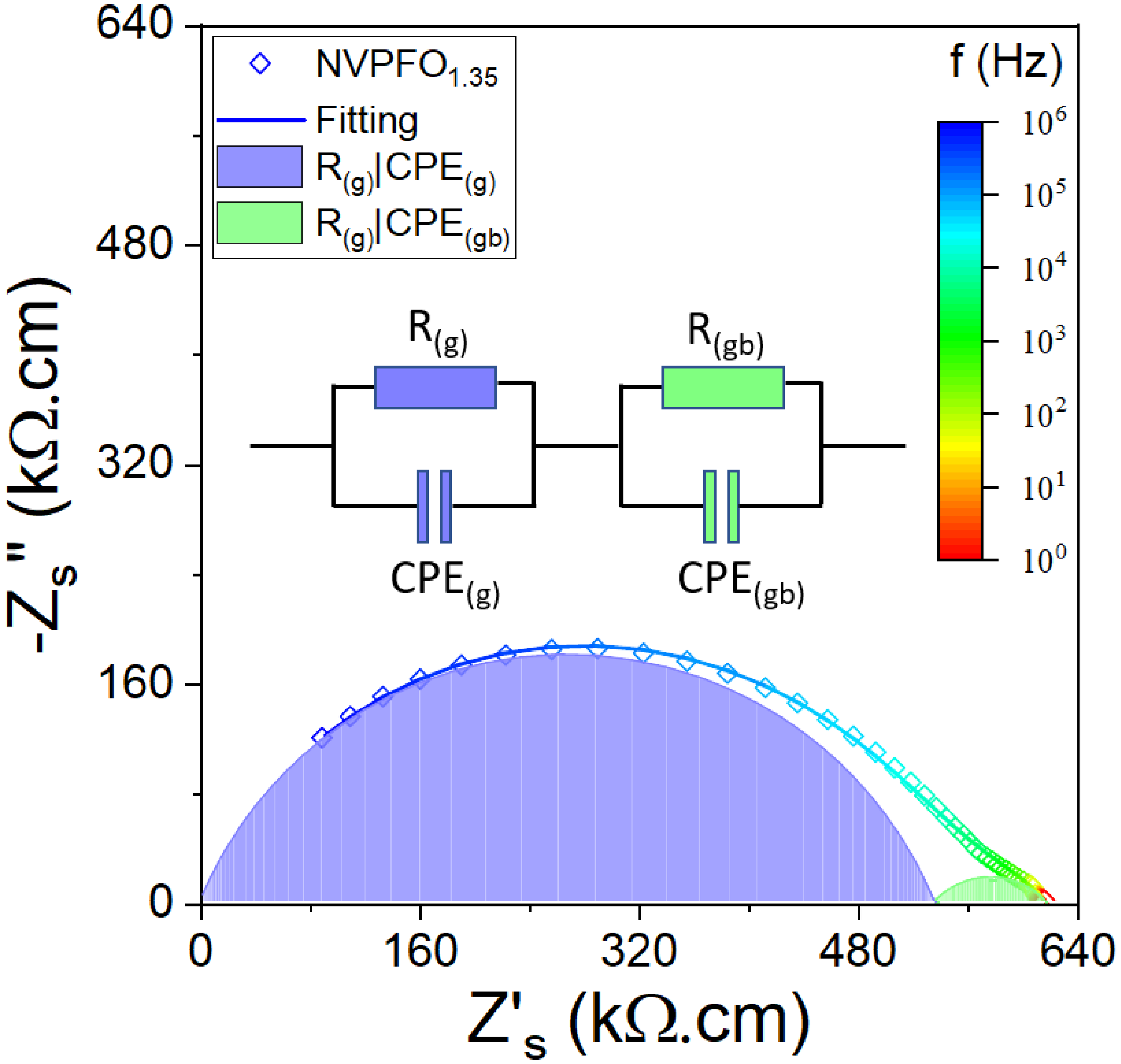


*Figure S10. Deconvolution of grain and grain boundary contributions of complex impedance data recorded at 200 ºC for NVPFO$_{1.35}$ sample. The complex impedance data shown here have already been normalized regarding the shape factor of the sample. The shown equivalent circuit is used for impedance data fitting. Acronyms R and CPE represent resistive and constant phase elements whereas g and gb stand for grain and grain boundary contributions, respectively. The obtained effective specific capacitances or the relative permittivities are typical from grain (1.4 pF.cm$^{-1}$ or 15) and grain boundary (470 pF.cm$^{-1}$ or 5329 [4]) contributions.*

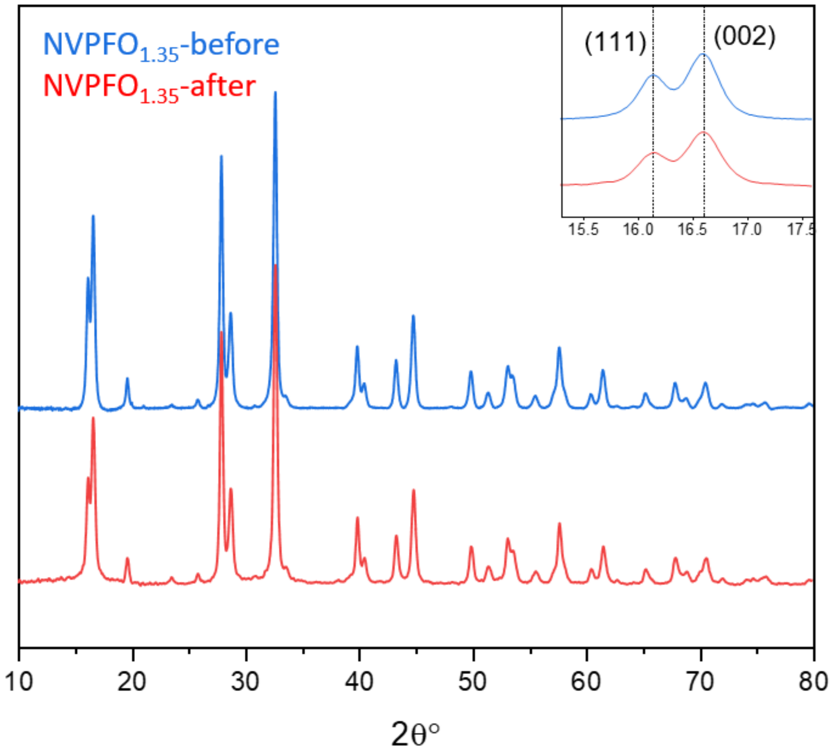


*Figure S11. Comparison of the XRD patterns collected for NVPFO$_{1.35}$, before and after the impedance measurement, with inset of enlarged (111) and (002) peaks.*

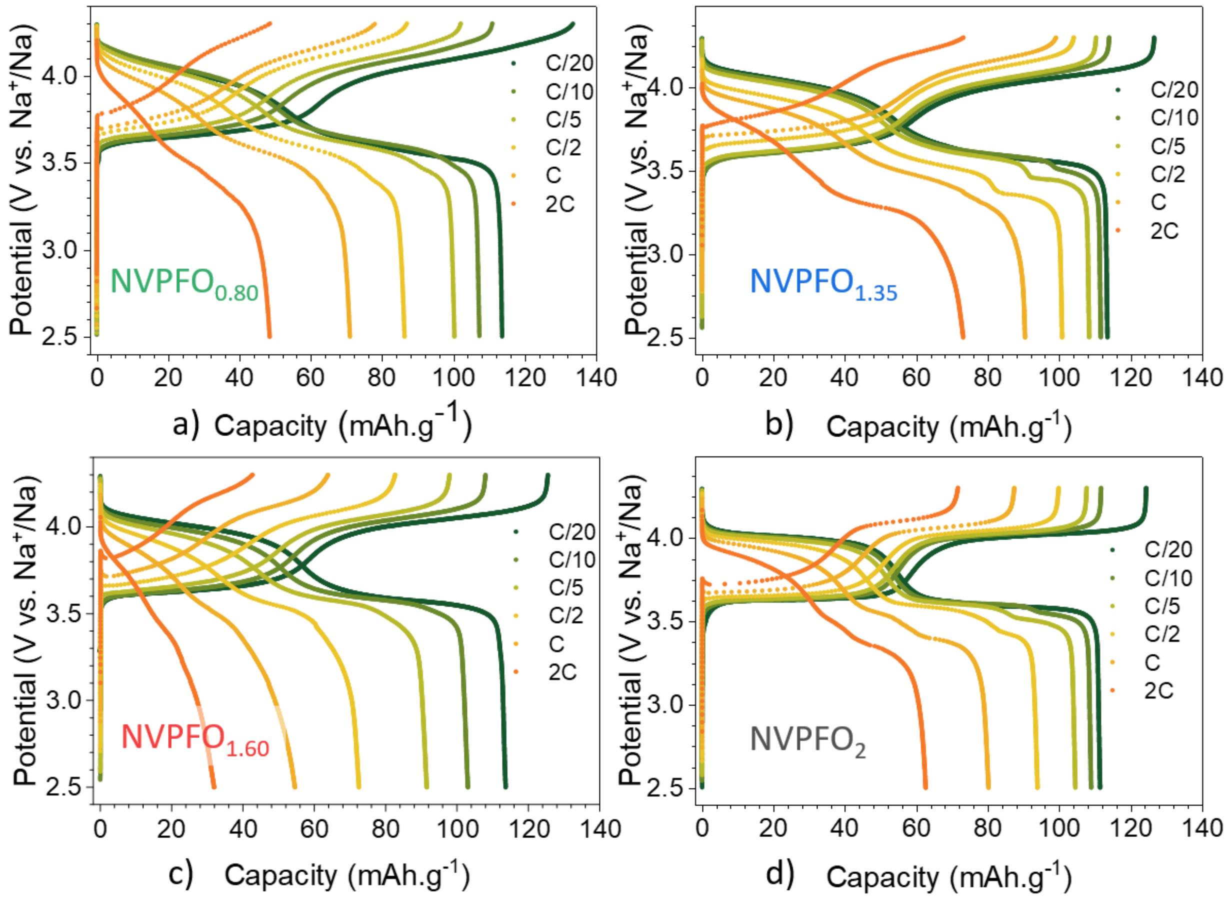


*Figure S12. Charge and discharge curves of $NVPFO_y$ materials at different cycling rates, from C/20 to 2C.*

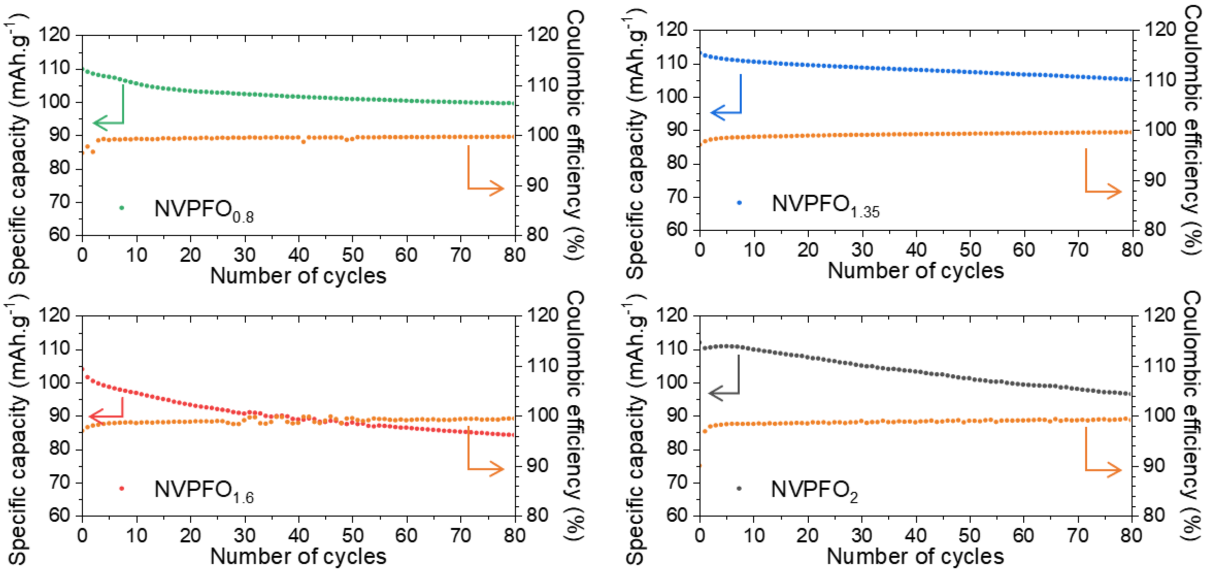


*Figure S13. Long range cycling performance (specific capacity and Coulombic efficiency) at C/10 for NVPFO$_y$.*

## Bibliography:


(1) Cai, Y.; Cao, X.; Luo, Z.; Fang, G.; Liu, F.; Zhou, J.; Pan, A.; Liang, S. Caging Na3V2(PO4)2F3 Microcubes in Cross-Linked Graphene Enabling Ultrafast Sodium Storage and Long-Term Cycling. *Adv. Sci.* **2018**, *5* (9). https://doi.org/10.1002/advs.201800680.

(2) Hall, N.; Boulineau, S.; Croguennec, L.; Launois, S.; Masquelier, C.; Simonin, L. Method For Ppreparing a Na3V2(PO4)2F3 Particulate Material. *United States Pat.* **2018**.

(3) Nguyen, L. H. B.; Broux, T.; Camacho, P. S.; Denux, D.; Bourgeois, L.; Belin, S.; Iadecola, A.; Fauth, F.; Carlier, D.; Olchowka, J.; Masquelier, C.; Croguennec, L. Stability in Water and Electrochemical Properties of the Na3V2(PO4)2F3 – Na3(VO)2(PO4)2F Solid Solution. *Energy Storage Mater.* **2019**, *20* (April), 324–334. https://doi.org/10.1016/j.ensm.2019.04.010.

(4) Irvine, J. T. S.; Sinclair, D. C.; West, A. R. Electroceramics: Characterization by Impedance Spectroscopy. *Adv. Mater.* **1990**, *2* (3), 132–138. https://doi.org/10.1002/ADMA.19900020304.